



NE-CAT COMMUNICATIONS



National Center for
Research Resources

A Biannual Newsletter of the Northeastern Collaborative Access Team Winter 2010

A Message from the Director Steven Ealick



Welcome to the latest edition of NE-CAT Communications, our biannual newsletter. Though the economic news from the mainstream media continues to be negative, NE-CAT concluded 2010 with good news in this area. I am happy to announce that we will be receiving funding from the Keck Foundation via a grant headed by one of our core

collaborators, Dr. David Eisenberg of UCLA. This grant will allow us to install a secondary focusing system on the micro-focus, fixed-energy beamline, 24-ID-E. This will not only enable us to achieve beam sizes smaller than 5 μm , but also will result in an increase in beam intensity, which will benefit all our users.

NE-CAT has also done well in other areas. Yet again, we see a higher number of overall publications in 2010 than in 2009. We end the year with 112 publications, an increase of 19% over last year. NE-CAT staff also co-authored 16 publications which shows the true collaborative nature of NE-CAT. I commend NE-CAT staffers for remaining active scientists and contributing extensively to current research.

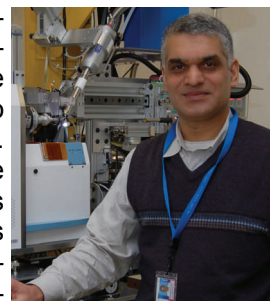
Another development worth mentioning here is that, on January 14, the Department of Health and Human Services (HHS) [informed](#) Congress of a plan to abolish NCRP and establish a new National Center for Advancing Translational Sciences. Currently, Congress has 180 days to respond to this proposal. The House appropriations subcommittee that oversees the HHS budget has not made a decision at this time. We have been reassured by our NCRP Program Contact, Mary Ann Wu, that no program will be terminated under this re-organization. As such, NE-CAT will maintain our current activities and continue to provide the best beamline facility and user support possible.

On a final note, the puck loan program mentioned in the last newsletter also has been very successful. Several user groups have participated in this program and found it to be very useful. If you have not used the sample automounter or visited NE-CAT recently, I encourage you to do so. For further information on our beamline

capabilities and how to request time, please visit our website at <http://necat.chem.cornell.edu>.

New NE-CAT Associate Director

The NE-CAT Executive committee has unanimously and enthusiastically decided to promote Kanagalaghatta Rajashankar to the position of Associate Director. Popularly known as Raj, he joined NE-CAT in 2005 and has been serving as the Operations Group Leader. He has been instrumental in developing the NE-CAT user program. He is also the



technical director of our core research on microdiffraction. In his new capacity, he will continue to be responsible for all beamline user activities, managing the user program and leading the staff scientists. Raj received his Ph.D. in 1997 and then worked at DESY and NSLS. At NE-CAT he has been one of the most prolific staff scientists, co-authoring many published works on crystallographically challenging biological problems.

Beamline Developments

1. RAPD

RAPD, our online data analysis environment presented in the last issue of our newsletter, has been moved off the beamline computers and onto the 128 core computing cluster. This allows a greater number of processes to run concurrently. Due to this move, we have changed our data integration from xia2 to a custom XDS-based pipeline. Previously, it was necessary to wait until the end of data collection before RAPD would integrate and scale data. Now data analysis is concurrent with data collection and users can observe data integration and scaling as images are collected.

RAPD has also received a SAD structure solution pipeline. The pipeline uses SHELX to search for and refine heavy atom positions and will attempt to autobuild the structure using PHENIX, placing in the sequence if it is provided by the user. A very useful tool in the pipeline is the unit cell analysis. It compares the observed unit cell from a data run to cell dimensions of structures deposited in the PDB. RAPD then reports if there are any

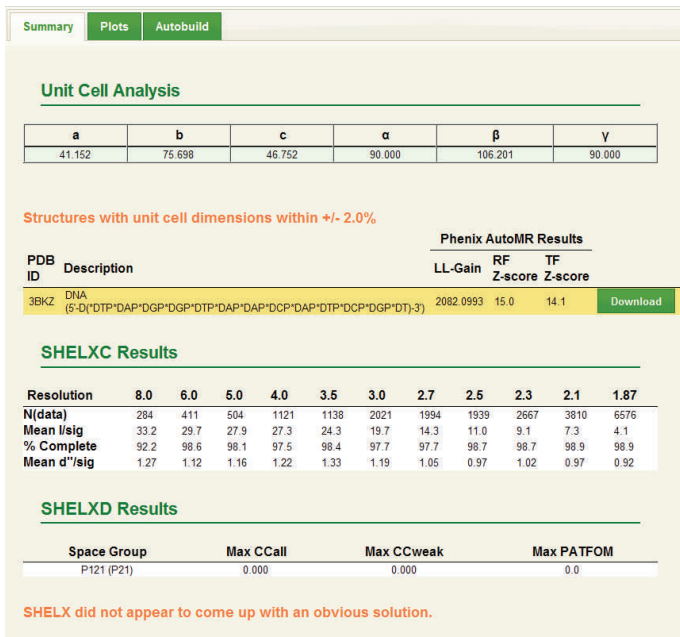


Fig. 1 SAD pipeline interface shows matches for unit cell in the PDB and SHELX results.

matches in the PDB. This can be highly informative if the wrong protein has been crystallized.

2. CONSOLE

The beamline software controls have also received many new capabilities. Prior to the fall 2010-3 run, it was necessary to use three separate interfaces on three separate computers to control the data collection software, the MD2 microdiffractometer, the robot and the beamline hardware. Control of data collection and the MD2 microdiffractometer has been integrated into our custom CONSOLE beamline control software. A single interface reduces exhaustion-induced confusion and simplifies use of the beamline. More importantly, this integration also allowed us to develop new forms of data collection that exploit the high precision and reproducibility of the MD2's x,y,z sample centering stages. These data collection methods make better use of crystals larger than the beam size and distribute X-ray damage over the entire volume of large crystals.

Vector Scanned Data Collection Modes

Many crystals studied at the NE-CAT beam lines are significantly larger than the apertured beam size provided by our MD2 microdiffractometers. The largest MD2 aperture available at the C- and E-lines is 100 μm in diameter, so unless multiple data collection runs, centered on different regions of the crystal are executed, most of the volume of larger crystals goes unutilized. We collectively refer to these new data collection protocols under the rubric of "Vector-Scanned" data collection. Vector-scanned data collection synchronizes displacements of the x, y and z sample centering stages of the MD2 with acquisition of the Q315 data frames, so

that, fresh parts of the crystal are brought to diffraction position for each frame during data collection.

Under vector scanned data collection, the user defines a 3-space scanning vector, spanning all or a section of a sample crystal by selecting two or more "3-click" alignment points across the crystal. 3-click alignment refers to the algorithm the MD2 control system uses to align a user-selected point, within a sample crystal, to the fiducial reference point in the MD2's inline visualizer video field (coincident with the X-ray beam). With rod or needle-like crystals, the scanning vector is usually aligned along to the long axis of the crystal.

Discrete Vector Scan

The Discrete Vector Scan mode (Fig. 2) partially distributes the effects of radiation damage over the run data. For each scan point, radiation damage accumulates at a fixed rotational-projection volume, corresponding to that scan point. However, since each scan point represents a single run data set, it is easy to cull aggregate data sets prior to final scaling with this scan method.

Continuous Vector Scan

The Continuous Vector Scan mode (Fig. 3) programs a single run sequence (all output files from the resultant run have the same prefix name and run number). Small x,y,z displacements along the scanning vector are executed after each Q315 data frame has been acquired. This method is useful for equi-partitioning radiation damage along the scanning vector.

Another benefit of vector-scanned data collection is the ability to distribute radiation damage across the scanned volume of large crystals. Comparison of data sets generated by vector scanning versus data sets collected at a single rotational point show that vector-scanned data sets have significantly higher statistical quality (lower B-factors, higher I/ σ , and lower R_{merge}).

RasterSnap

The "RasterSnap" vector-scanning procedure (Fig. 4) is used to locate the best diffractive region of large, possibly inhomogeneous crystals. The RasterSnap dialog programs a set of snapshot data frames, along the scanning vector, to be acquired with fixed data collection parameters (including omega). The DISTL component of RAPD is used to calculate a series of diffraction quality metrics. A summary of the diffraction metrics is displayed and the user can use this dialog to plot a selected subset of the metrics as a function of scan position index. If a maximum is found in one or more of the diffraction metric traces, the user can select a data record in the scan point dialog that causes the MD2 x,y,z centering stages step to the selected scan point coordinates, for further data collection.

Diffractive Alignment

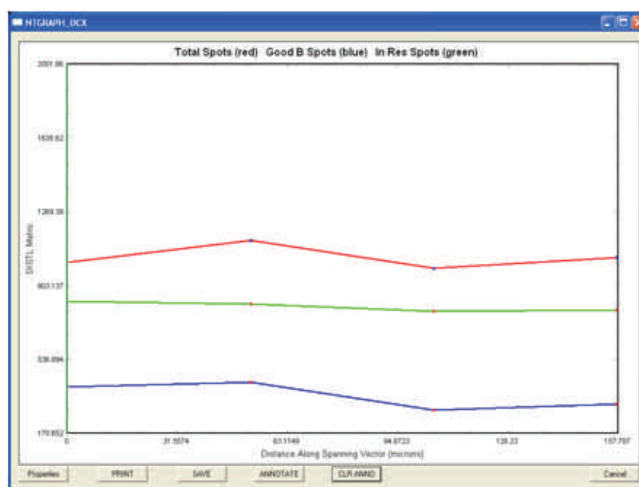
Another data collection protocol has been developed for



Fig. 2 View of discrete vector scan configuration, overlain on a still frame of the sample. The yellow line is a projection of the scanning vector. Red ellipses indicate beam size at each selected scan point.



Fig. 3 View of continuous vector scan configuration, overlain on a still frame of the sample. The yellow line is a projection of the scanning vector. Red ellipses indicate beam size at each selected scan point.



Raster Snap DISTL Results

	<input type="checkbox"/> DISTL Res	<input type="checkbox"/> LABELIT Res	<input type="checkbox"/> Overloads	<input type="checkbox"/> Total Spots	<input type="checkbox"/> Good B Spots	<input type="checkbox"/> In Res Spots	<input type="checkbox"/> Max Signal	<input type="checkbox"/> Mean Signal	<input type="checkbox"/> Min Signal
1	2.5000	2.2700	0	1021	402	826	0.0000	0.0000	0.0000
2	2.3600	2.3300	0	1130	425	814	0.0000	0.0000	0.0000
3	2.6000	2.2700	0	992	289	778	0.0000	0.0000	0.0000
4	2.3300	2.2600	0	1044	316	785	0.0000	0.0000	0.0000

EXIT PLOT MOVETO

Fig. 4 RasterSnap diffraction quality analysis returns. Upper Left: configuration window. Upper Right: trace window of DISTL metrics. Lower: Result Selector dialog for controlling which DISTL metrics are plotted (row of check boxes at top of dialog). By selecting a row in the Result Selector dialog corresponding to a scan point and striking the MOVETO button, the MD2 centering stages will align the selected scan point to the alignment fiducial.

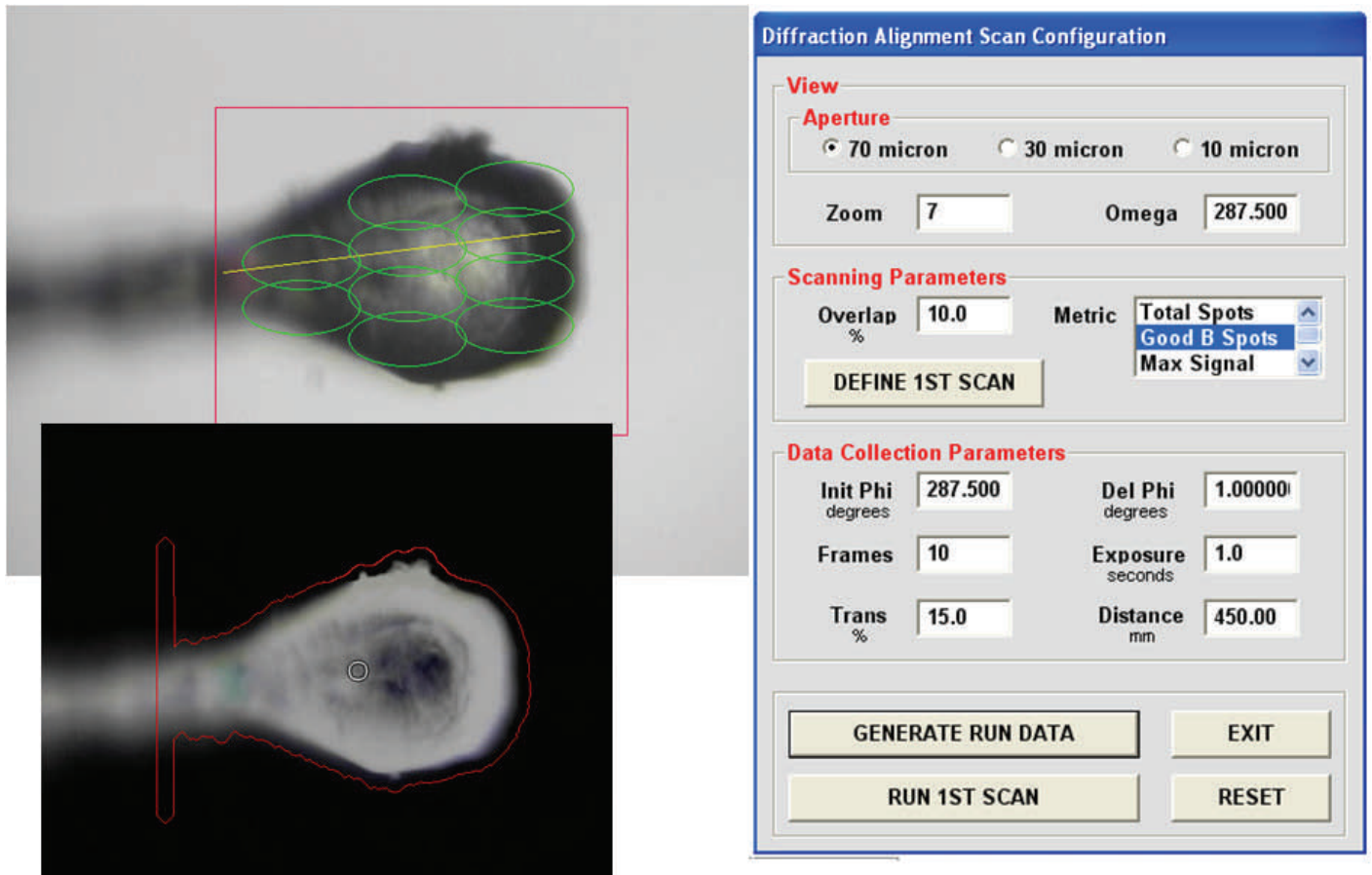


Fig. 5 Diffractive alignment Auxiliary Console script dialog (right) and configuration windows for this method (left). The lower left window shows a crystal trapped in semi-opaque cryosolution due to presence of precipitant. Green ellipses in the upper left panel represent the positions used in the first scan.

automatic centering of crystal mounts in which the sample cannot be clearly visualized, due to frost accumulation or opaque, frozen cryosolution and more importantly, for membrane proteins crystallized in a lipid cubic phase. Figure 5 shows the constructor dialog for the diffractive alignment protocol.

In this method, individual snapshots are automatically taken by the protocol within a pre-defined area. Through integration with RAPD, the DISTL package is used for identifying Bragg spots in the snapshots and a metric is calculated to predict the "best" spot. A single scan allows for determination of a crystal within an opaque matrix. Two scans allow the system to re-

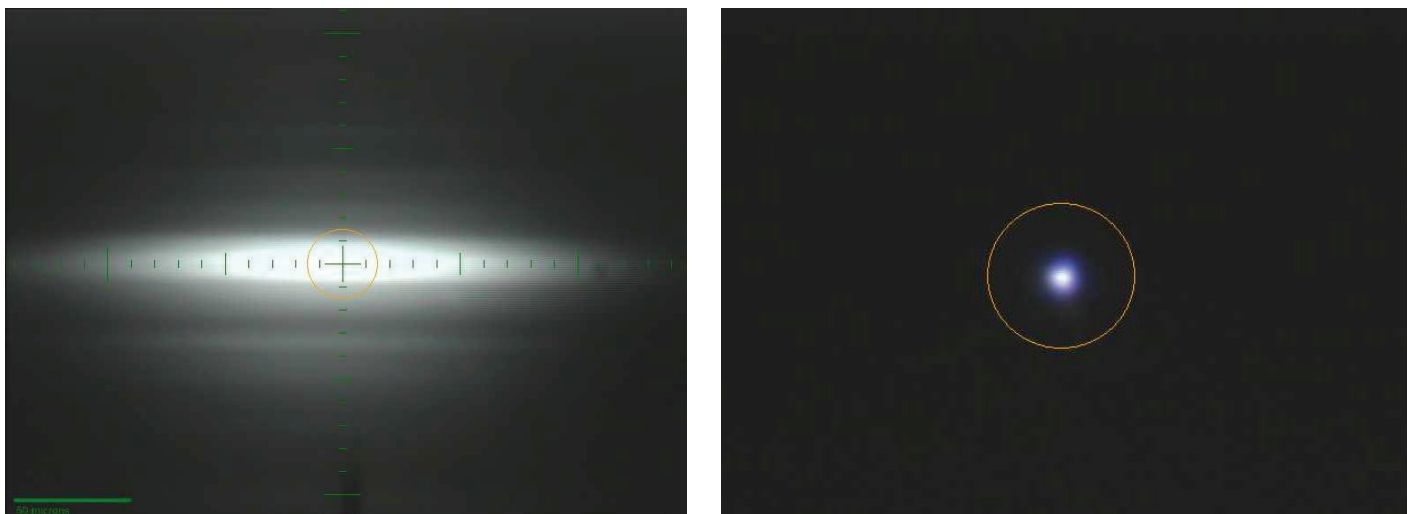


Fig. 6 On the left is an attenuated, focused beam imaged by MD2 scintillation screen. On the right is the shaped beam imaged by MD2 scintillation screen, using a 5 μm diameter aperture and a 100 μm diameter scatter guard. Orange-colored fiducial marks in both figures are 25 μm in diameter.

center on the centroid (x,y,z) for the “best” spot.

3. Compound Refractive Lens

Currently, NE-CAT’s 24-ID-E beamline optics provide monochromatic X-rays at a single, fixed energy (12662.0 KeV) and are dedicated to microdiffraction. Focusing at 24-ID-E is effected via conventional Kirkpatrick-Baez optics and achieves a spot size of 15 x 100 μm, 3 sigma (Vertical x Horizontal), with a total flux of 1 x 10¹³ photons/sec (without aperture).

On 24-ID-E, circular apertures are used to create beam sizes smaller than 15 x 100 μm but the apertures act as shaping masks. Therefore, the available flux outside of the area produced by the aperture is blocked from passing through the aperture hole and is not available. This means a smaller aperture size equals reduced flux on the crystal. As a result, it is necessary to expose crystals in the 5 μm beam longer in order to achieve the same radiation dose.

In order reduce the size of the beam in the horizontal and increase flux levels, NE-CAT will be installing a Compound Refractive Lens (CRL) on 24-ID-E. A CRL is actually not a single lens, but a series of individual lenses arranged in a linear array. The lenses are beryllium blocks drilled with cylindrical holes.

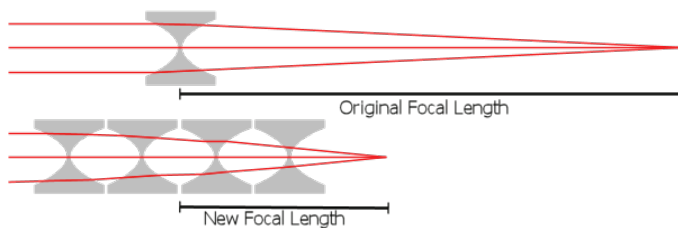


Fig. 7 How a CRL works. Grey shapes are individual lenses. The bottom diagram shows how a CRL shortens the focal length when it replaces a single lens.

The array allows the focusing of X-rays and reduces the focal length of the beam. The intent of installing a CRL on 24-ID-E is to reduce the width of the beam in the horizontal and subsequently increasing the available flux in the centroid of the beam.

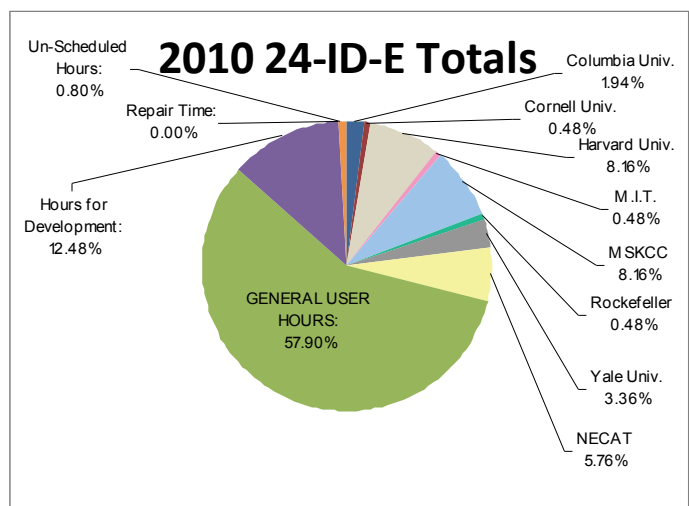
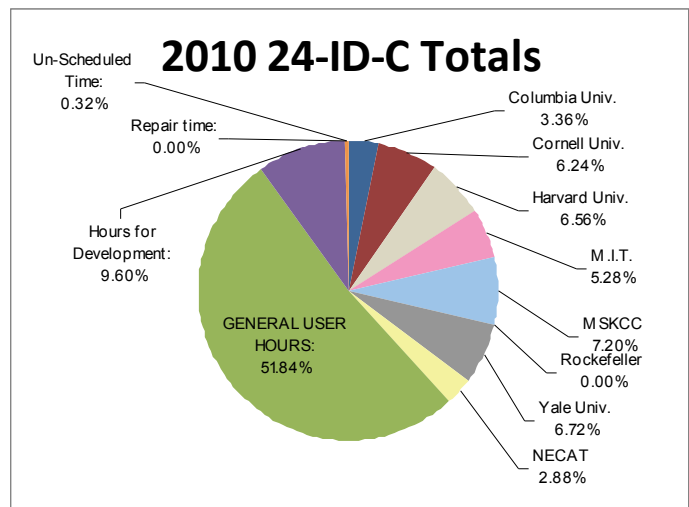
We propose to improve the focusing capability of 24-ID-E by installing a secondary focusing system just upstream of the existing MD2 microdiffractometer, at the waist of the current monochromatic beam. This secondary focusing system will consist of a beryllium CRL. A precision positioning system will be developed for the secondary focusing optic, installed on a vibration isolation table to mitigate the potential effects of mechanical perturbations arising from the APS floor. With the proposed secondary focusing optics, we hope to achieve a focus spot under one micron, with an increased flux density of one order of magnitude. This will be done via funding from the Keck Foundation via a grant to one of

our core collaborators, Dr. David Eisenberg of UCLA.

Use of NE-CAT Beamlines

Per our promise to NCCR, we are required to provide at least 50% of our available beamtime to APS general users. As can be seen in the pie charts, during 2010 we exceeded this expectation. General user subscription on 24-ID-C was 52% and 24-ID-E was 58%. However, this was done without affecting NE-CAT members. Un-used member time is allocated to general users.

The puck loan program mentioned in the 2010 Summer Newsletter has been very successful. In 2010, we loaned out 27 sets of pucks to 24 labs. In addition, ~160 pucks were borrowed and loaded on-site using our NE-Puck Loader. All users who are interested in taking advantage of the sample automounter are encouraged to participate. Further details on the sample automounter and the puck loan program can be found at <http://lilith.nec.aps.anl.gov/~perry/index.html>.



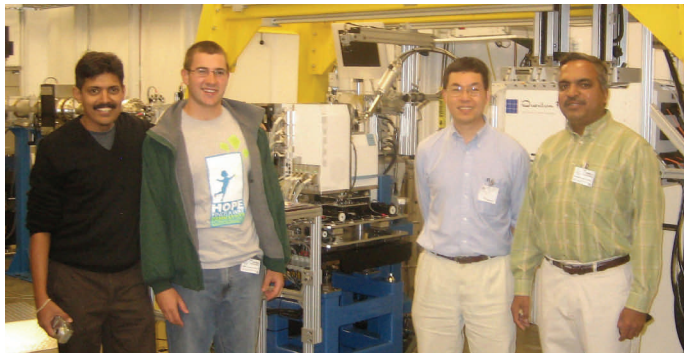


Fig. 8 The Penn State team of Ravindra Makde, Joe England, Song Tan and Hemant Yennawar (from left to right).

Research Highlights

Structure of RCC1 chromatin factor bound to the nucleosome core particle

Song Tan, Penn State, Department of Biochemistry and Molecular Biology, University Park, PA

Each cell in our body contains about 2 meters of DNA that has to fit into a nucleus about 10 micrometers in diameter. This compaction is achieved by wrapping the DNA around histone proteins into what is known as chromatin. For a long time, chromatin was thought to be a repressive structure whose main function was to repress gene expression. However, it is now recognized that chromatin is an active participant in both the activation and repression of gene expression, and that this participation is mediated by chromatin enzymes. The interaction between chromatin enzymes and the nucleosome (the fundamental repeating unit of chromatin) is therefore central to gene regulation, and yet the molecular basis for this interaction was not known.

Song Tan and his colleagues at Penn State University have worked on the structural question of how chromatin enzymes or proteins bind to the nucleosome over the last 9 years. The initial challenge was to produce recombinant nucleosome core particles (200 kDa protein-DNA complex of 4 core histones and about 150 bp of DNA), and to reconstitute these with chromatin enzymes to produce a homogeneous complex. The next hurdle was to grow crystals of such chromatin enzyme/nucleosome complexes. A major breakthrough occurred when Tan's lab was able to grow crystals of the nucleosome in complex with the RCC1 protein critical for proper segregation of chromosomes during cell division. Over a span of about a year and a half, postdoctoral fellow Ravindra Madke was able to improve the initial crystals by using different RCC1 orthologs and, critically, by careful optimization of post-crystallization soaks to dehydrate the crystals.

The RCC1-nucleosome crystals were initially character-

ized at X-ray diffraction beamline A1 at the Cornell High Energy Synchrotron Source (CHESS), and further diffraction analysis was performed at the Northeastern Collaborative Access Team (NE-CAT) facility at the Advanced Photon Source (APS). The NE-CAT 24-ID-E beamline with its highly focused and brilliant beam proved to be critical to successful diffraction data collection of the 300 kDa RCC1-nucleosome complex crystals to 2.9 Å resolution. This data was used to determine the first atomic structure of a chromatin protein bound to the nucleosome. The structure, solved by molecular replacement, shows that the beta-propeller RCC1 protein recognizes the architecture of the nucleosome by interacting with both histone and DNA components. The manuscript describing this work was recently published in *Nature* (Makde et al, *Nature*, 467:562-566, 2010).

NE-CAT personnel played a major role in the success of the project. Song Tan said, "We are grateful to the entire NE-CAT staff for creating and maintaining this world-class facility. The superb technical support

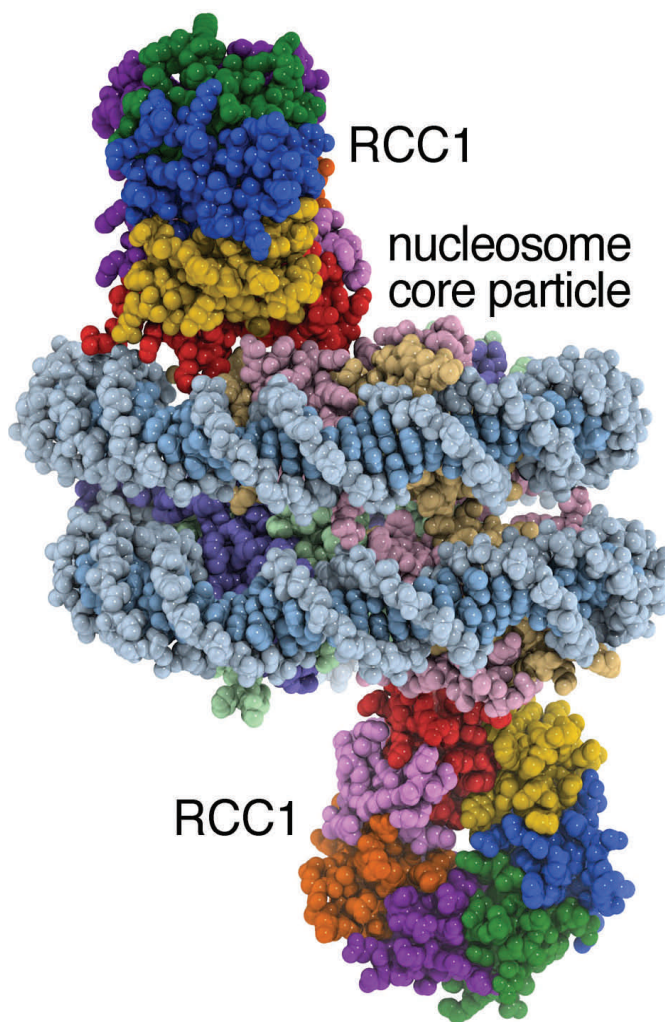


Fig. 9 Crystal structure of the 300 kDa RCC1-nucleosome core particle complex shown in space filling representation. Figure prepared in PyMol.

we received allowed us to collect the best possible diffraction data from our crystals.”

Structure and mechanism of a bacterial urea transporter.

Ming Zhou, Columbia University Medical Center, Department of Physiology and Cellular Biophysics, New York, NY



One of the necessary adaptations required for terrestrial animals to survive on dry land is the ability to maintain constant internal osmolarity and fluid volume in the face of intermittent access to water. In mammals, water homeostasis is achieved largely by the kidneys, which can regulate water excretion by varying degrees in balance with water intake. The mechanism for water re-absorption is dependent in part on an extremely high concentration of the metabolic waste product urea in the medullary interstitium. Because unassisted urea diffusion through lipid bilayers is extremely slow, the cells of the inner medullary collecting ducts express integral membrane proteins known as urea transporters (UT) to facilitate the rapid flux of urea essential for water re-absorption (Knepper and Star, 1990). All UTs conduct urea, but different homologs range in selectivity; while some permit water and a variety of urea analogs, the most stringent homologs characterized thus far have only been shown to conduct urea, excluding even smaller urea analogs such as formamide (Maciver et al., 2008).

To better understand how UTs achieve the rapid and selective flux of a highly polar molecule across the membrane, we set out to solve the structure of a member of the UT family. As part of our involvement with the New York Consortium on Membrane Protein Structure (NYCOMPS), we screened a number of bacterial UT homologs for overexpression and crystallization, and identified a suitable candidate from the bacterium *Desulfovibrio vulgaris*, dvUT. In total, we screened over 500



Fig. 10 Postdoctoral fellow Elena Levin in the Zhou Lab performed the pertinent structural studies.

crystals of dvUT, an effort that included extensive use of the NE-CAT beamlines. Eventually, we were able to obtain a 2.3 Å dataset from a crystal derivatized with gold cyanide, and solved the structure by SAD (Levin et al., 2009).

The crystal structure of dvUT reveals that the protein is a trimer (Figure 11a), and each protomer contains two homologous halves that adopt a similar fold with an inverse orientation in the membrane, so that each subunit has a pseudo-twofold rotational symmetry axis parallel to the membrane. The two halves of the protein each contain five transmembrane helices and one half membrane spanning helix, tilted at a roughly 45° angle relative to the membrane normal. Each protomer contains a membrane-spanning, solvent accessible pore at the center of the interface between the two related halves (Figure 11b).

We reasoned that dvUT was in fact a channel rather than a transporter, and these pores represented the permeation pathway for urea. To confirm that this pathway represents the channel pore, we attempted to co-crystallize dvUT with urea and a variety of urea analogs. While so far we have been unsuccessful at obtaining a high-resolution urea-bound structure, we were able to solve a 2.4 Å structure of dvUT bound to the urea analog 1,3-dimethylurea (DMU). Two clear electron density peaks appear in the pore, allowing the placement of DMU with an unambiguous orientation (Figure 11c-d). The two DMU molecules mark the ends of a constricted region roughly 14 Å long in the middle of the pore that we refer to as the channel's selectivity filter.

Perhaps the most striking feature of the selectivity filter is a linear row of oxygen atoms contributed by backbone carbonyls and side chains running along the length of one side (Figure 11e). These oxygens are located at the ends of the two half-membrane spanning helices, which are oriented with their helix dipoles pointing towards the filter. In the ligand-bound structure, both DMU molecules are located with their amino groups positioned to form hydrogen bonds to these “oxygen ladders”. The oxygen ladders are reminiscent of the selectivity filters of K⁺ channels, which replace ion coordination waters with carbonyl oxygens whose electronegativity is strengthened by their location on the ends of helix dipoles (Doyle et al., 1998). The other residues lining the selectivity filter are hydrophobic, with two notable exceptions: a pair of highly conserved threonine residues at a constriction near the center of the pore. The pore is rectangular in cross-section, particularly at the two observed DMU binding sites, where pairs of co-facial phenylalanine residues form a tight fit against the plane of the DMU molecules.

From these observations of the dvUT structure, we have been able to propose a tentative mechanism for how UTs permeate urea. Helix dipole-strengthened hydrogen

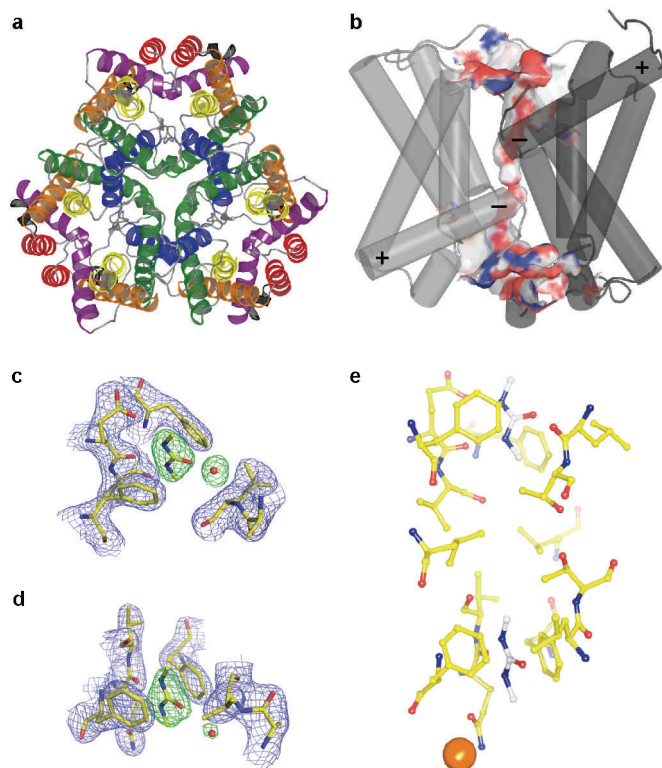


Fig. 11 (a) The dvUT trimer. (b) A dUT protomer with the pore shown as a surface and the dipoles of the tilted helices marked. (c-d) The binding sites for DMU shown with the 2Fo-Fc density shown in blue and contoured at 1.5σ and Fo-Fc density calculated without the ligand shown in green and contoured at 3σ . (e) The selectivity filter of dvUT shown bound to DMU. The orange sphere shows the location of a gold atom.

bonds between the oxygen ladders and the urea amino groups likely compensate for the loss of interactions with water as dehydrated urea molecules move along the pore. Permeating urea is further stabilized by hydrophobic interactions with the walls of the pore, which are shaped to neatly match the shape and dimensions of urea. The role of the conserved threonine residues is less clear, and will be one focus of future functional studies of the mechanism of UT permeation and selectivity.

References

- Doyle, D.A., Morais Cabral, J., Pfuetzner, R.A., Kuo, A., Gulbis, J.M., Cohen, S.L., Chait, B.T., and MacKinnon, R. (1998). The structure of the potassium channel: molecular basis of K^+ conduction and selectivity. *Science* **280**, 69-77.
- Knepper, M.A., and Star, R.A. (1990). The vasopressin-regulated urea transporter in renal inner medullary collecting duct. *Am J Physiol* **259**, F393-401.
- Levin, E.J., Quick, M., and Zhou, M. (2009). Crystal structure of a bacterial homologue of the kidney urea transporter. *Nature* **462**(7274), 733-4.

Maciver, B., Smith, C.P., Hill, W.G., and Zeidel, M.L. (2008). Functional characterization of mouse urea transporters UT-A2 and UT-A3 expressed in purified *Xenopus laevis* oocyte plasma membranes. *Am J Physiol Renal Physiol* **294**, F956-964.

Staff Activities

Posters

Jon Schuermann, David Neau, Kanagalaghatta Rajashankar, Frank Murphy, "Rapid Automated Processing of Data (RAPD) Software Package," P41 Principal Investigator Meeting: "Omics," Data Sharing, and Translational Research, Rockville, Maryland, October 12-13, 2010.

Publications

- Demirci, H., Murphy, F. V. IV, Belardinelli, R., Kelley, A. C., Ramakrishnan, V., Gregory, S. T., Dahlberg, A. E., and Jogl, G. (2010) Modification of 16S ribosomal RNA by the KsgA methyltransferase restructures the 30S subunit to optimize ribosome function, *RNA* **16**, 2319-2324.
- Singh, H., Schuermann, J. P., Reilly, T. J., Calcutt, M. J., and Tanner, J. J. (2010) Recognition of Nucleoside Monophosphate Substrates by *Haemophilus influenzae* Class C Acid Phosphatase, *J. Mol. Biol.* **404**, 639-649.
- Bale, S., Rajashankar, K. R., Perry, K., Begley, T. P., and Ealick, S. E. (2010) HMP Binding Protein ThiY and HMP-P Synthase THI5 are Structural Homologues, *Biochemistry* **49**, 8929-8936.
- Long, F., Su, C.-C., Zimmermann, M. T., Boyken, S. E., Rajashankar, K. R., Jernigan, R. L., and Yu, E. W. (2010) Crystal structures of the CusA efflux pump suggest methionine-mediated metal transport, *Nature* **467**, 484-488.

Acknowledgements

NE-CAT is supported by Grant (RR-15301) from the NIH National Center for Research Resources and contributions from the following NE-CAT institutional members:

Columbia University
 Cornell University
 Harvard University
 Massachusetts Institute of Technology
 Memorial Sloan-Kettering Cancer Center
 Rockefeller University
 Yale University